JOURNAL OF GEOPHYSICAL RESEARCH, VOL. 115, D07103, doi:10.1029/2009JD012726, 2010

Response of OH airglow temperatures to neutral air dynamics at 78°N, 16°E during the anomalous 2003–2004 winter

M. E. Dyrland,[1] F. J. Mulligan,[2] C. M. Hall,[3] F. Sigernes,[1] M. Tsutsumi,[4] and C. S. Deehr[5]

Received 24 June 2009; revised 17 November 2009; accepted 7 December 2009; published 8 April 2010.

[1] Hydroxyl (OH) brightness temperatures from the mesopause region derived from temperature profiles from the Sounding of the Atmosphere using Broadband Emission Radiometry (SABER) instrument on the Thermosphere, Ionosphere, Mesosphere Energetics and Dynamics (TIMED) satellite are compared with OH(6-2) rotational temperatures measured by spectrometer from Longyearbyen, Norway (78°N, 16°E), during the winter 2003–2004. The two series correspond well, although the satellite measurements are higher by an average of 5.6 K ± 4.4 K. Reasons for this apparent bias are discussed. The two series give a near-continuous temperature record from this winter, making it possible to study the response of the temperatures to neutral air dynamics observed from meteor radar measurements of meridional and zonal wind. Vertical profiles of 1.6 μm OH volume emission rates from SABER reveal that the unusually high temperatures observed during January and February 2004 (240–250 K) correspond to a very low and bright OH layer. Significant linear correlations are found between meridional wind, OH temperature, and peak altitude. These data support the theory that the high temperatures result from an anomalously strong upper stratospheric vortex that confined air to the polar regions, coupled with meridional transport, which led to a strong downwelling of atomic oxygen-rich air, thereby lowering the altitude of the OH layer. The SABER data reveal that the re-formation of the OH layer at approximately 78 km altitude accounted for an increase in temperature of approximately 15 K, while the remaining temperature increase (20–35 K) is attributed to adiabatic heating and chemical heating from the exothermic reactions involved in producing the vibrationally excited OH.

Citation: Dyrland, M. E., F. J. Mulligan, C. M. Hall, F. Sigernes, M. Tsutsumi, and C. S. Deehr (2010), Response of OH airglow temperatures to neutral air dynamics at 78°N, 16°E during the anomalous 2003–2004 winter, *J. Geophys. Res.*, *115*, D07103, doi:10.1029/2009JD012726.

1. Introduction

[2] The Arctic winter of 2003–2004 has been reported as remarkable from several points of view and has been the subject of many studies. *Manney et al.* [2005] described how a disruption of the polar vortex and an associated sudden stratospheric warming (SSW) persisted at the low and middle stratosphere throughout the entire winter, while the upper stratospheric vortex quickly reformed in mid January and became the strongest on record by mid February. This resulted in anomalously high temperatures in the lower and middle stratosphere and an unusually cold upper stratosphere.

[3] At the upper mesospheric level, the dominant circulation pattern during an Arctic winter consists of eastward directed zonal winds (westerlies) and poleward meridional flow from summer pole to winter pole [*Andrews et al.*, 1987]. During SSW events, gravity and planetary waves disrupt the polar stratospheric vortex, which leads to a warming of the stratosphere of up to 70 K at the 10 hPa level (~30 km) [*Schoeberl*, 1978] and to a reversal of the mean zonal wind in the case of a major SSW. The large-scale effects of the SSW on the mesospheric temperature and wind field for the 2003–2004 winter were studied by *Shepherd et al.* [2007] and *Mukhtarov et al.* [2007] for latitudes ranging from the tropics up to 70°N. They observed a reduction of the upper mesospheric temperature and a reversal of the zonal wind that preceded the changes in the stratosphere. This is consistent with previous studies of stratospheric warming/mesospheric cooling events made by use of ground-based optical measurements of hydroxyl (OH) rotational temperatures, models, and radars [e.g., *Walterscheid et al.*, 2000; *Hoffman et al.*, 2007]. The implication is that there is a

[1]The University Centre in Svalbard, Longyearbyen, Norway.
[2]Department of Experimental Physics, National University of Ireland, Maynooth, Ireland.
[3]Tromsø Geophysical Observatory, University of Tromsø, Tromsø, Norway.
[4]National Institute of Polar Research, Tokyo, Japan.
[5]Geophysical Institute, University of Alaska Fairbanks, Fairbanks, Alaska, USA.

0148-0227/10/2009JD012726

downward propagation from the mesosphere-lower thermosphere (MLT) to the stratosphere. However, other authors have found no correlation between stratospheric temperatures and the rotational temperature of the OH Meinel band at ~87 km [*Siskind et al.*, 2005], indicating that there might be an altitude limit to how far these events affect the atmosphere or that other features of the OH layer dynamics hide the variations. It is important, therefore, to continue to study these events in order to obtain a more complete understanding of the processes causing them.

[4] Rotational temperatures derived from optical measurements of the OH Meinel airglow bands in the spectrum of the night sky have been used extensively as a proxy for the neutral temperature in the uppermost part of the mesosphere, the so-called mesopause region (80–100 km) [*Beig et al.*, 2003, and references therein]. Temperatures derived from spectrometric measurements of the OH(6-2) Meinel band measured above Longyearbyen, Svalbard, Norway (78°N, 16°E), comprise one of the longest records of mesopause region temperatures in the world [*Sigernes et al.*, 2003]. In a paper giving an update on this temperature series *Dyrland and Sigernes* [2007] reported unusually high OH(6-2) rotational temperatures for the 2003–2004 season compared to the whole series from the early 1980s to 2005. In a recent paper, *Winick et al.* [2009] noted that while several authors documented abnormal conditions of various sorts in the 2003–2004 winter, none of these conditions were related specifically to OH. Using data from the Sounding of the Atmosphere using Broadband Emission Radiometry (SABER) instrument on the Thermosphere, Ionosphere, Mesosphere Energetics and Dynamics (TIMED) satellite, they gave a global picture of the OH layer characteristics from late January through February 2004 and showed that the very high OH temperatures were correlated with an unusually low and bright OH layer that exhibited significant zonal asymmetries. They argued that the lowered OH layer was due to the anomalously strong upper stratospheric vortex that formed after the SSW. The vortex supported increased downwelling of oxygen-rich air and displaced the OH layer to a lower altitude than normal. However, their study was limited by the period of time that SABER was viewing northward and could thus only report OH temperatures and heights from mid January 2004, thereby missing the actual time prior to and during the SSW.

[5] In this paper we examine OH temperature variability as measured by a ground-based spectrometer during the Arctic polar night of 2003–2004 and combine the data with SABER measurements to make a complete temperature record for this season. Supported by mesopause region wind data obtained by meteor radar from the same site, we establish the impact of the unusual atmospheric conditions on the OH layer and relate it to the neutral air dynamics observed above the high-latitude location Longyearbyen (78°N). We identify the time of onset of the high temperatures and compare the observations with current theories of the dynamics at high latitudes. Using OH layer peak altitudes and OH brightness-weighted temperatures derived from SABER measurements, we quantify the effect the lowering of the layer had on the temperature. For the first time, rotational temperatures derived from the OH(6-2) band are compared with satellite temperatures measured by SABER at such a high latitude.

2. Instruments and Data Retrieval

[6] The main data presented in this paper are temperatures retrieved from OH(6-2) spectra measured by a ground-based spectrometer, OH brightness temperatures, and OH layer peak altitudes measured by the satellite instrument SABER and zonal and meridional winds measured by the Nippon/Norway Svalbard Meteor Radar (NSMR). The following paragraphs provide a short overview of and references to the instruments and data retrieval.

[7] The OH(6-2) spectra are measured above Longyearbyen (78°N, 16°E). The Ebert-Fastie spectrometer used to obtain these spectra, the theory and practice behind the temperature retrieval, and the temperature series (1980–2005) have been thoroughly described and discussed [e.g., *Sivjee and Hamwey*, 1987; *Sigernes et al.*, 2003]. We will therefore only briefly describe the procedures here. The temperatures are derived from the measured intensities of certain rotational lines of the OH(6-2) vibrational band. The lines used for the analysis are the $P_2(2)$ to $P_1(5)$ lines, which are positioned in the wavelength range 8374–8512 Å. The analysis procedure consists in finding the background and a synthetic spectrum that best fit the measured spectrum [*Sigernes et al.*, 2003]. The temperature can be derived from the slope of a linear fit to the P_1 lines in a so-called Boltzmann plot (log-energy term plot). The error in the slope of the fit of each hourly averaged spectrum is used to compute the measurement uncertainty in the derived temperature. Typical uncertainties estimated by this procedure are ~8 K for temperatures derived from hourly averaged OH (6-2) spectra. Spectra contaminated by aurora or scattered city lights or moonlight are discarded from the analysis. Some changes have been made to the analysis since the report of *Dyrland and Sigernes* [2007]. For the present study the transition coefficients used in the temperature retrieval have been changed to those calculated by *Goldman et al.* [1998]. This change relative to previous analyses of data from Longyearbyen is based on the study of *Cosby and Slanger* [2007], who concluded that the *Goldman et al.* [1998] set yielded values that were most consistent with their calibrated emission intensities.

[8] Daily averaged OH(6-2) temperatures were calculated from days that had at least three hourly averages available. The daily averaged OH(6-2) temperatures from 2003 to 2004 are shown in green in Figure 1 (top). The error bars are the standard deviation of the individual measurements comprising the daily mean. It is important to note that these are mainly governed by atmospheric variability, but they also encompass the uncertainty of the temperature retrieval (~8 K). Alternatively we could have followed *Bevington and Robinson* [1992] and calculated the daily mean and uncertainty in the daily mean by weighting the hourly averaged temperatures according to their individual uncertainty. However, since we do not have the individual uncertainties available for the SABER data, we choose to weight the hourly means equally for both the OH(6-2) and SABER data and use the standard deviation from the mean to indicate the error.

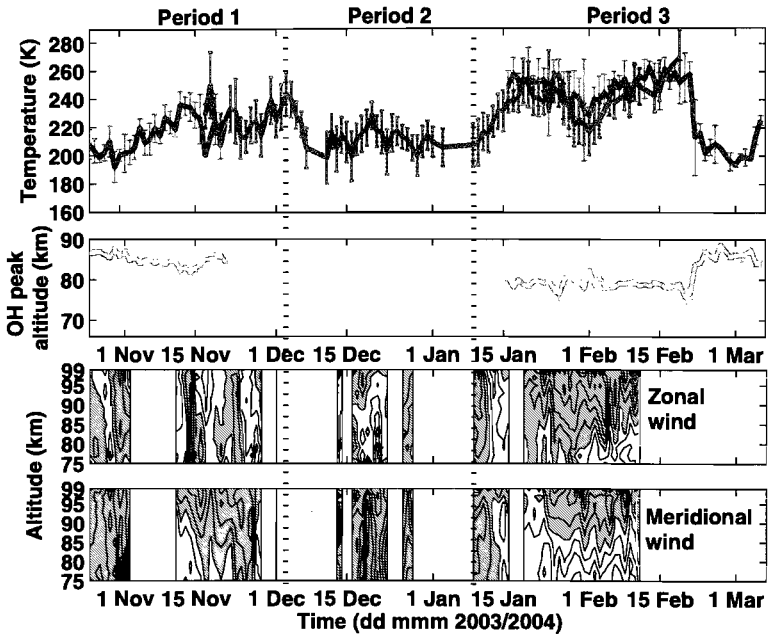

Figure 1. (top) OH(6-2) temperatures from Longyearbyen (78°N, 16°E) and OH brightness temperatures from the Sounding of the Atmosphere using Broadband Emission Radiometry (SABER) instrument (version 1.07) at 78 ± 5°N, 16 ± 10°E for the winter season 2003–2004. Daily mean OH(6-2) temperatures and SABER temperatures are shown in green and dark blue, respectively. (middle) Daily averaged SABER OH peak altitudes. (bottom) Zonal winds measured by the NSMR meteor radar binned in 2 km bins from 74 to 100 km and daily averaged (white indicates eastward winds, gray indicates westward winds, and contour lines are shown for levels of 20 m/s), and meridional winds measured for the same ranges as the zonal wind (white indicates poleward winds, and gray indicates equatorward winds).

[9] While OH(6-2) temperatures represent a type of weighted average over the OH layer, which has a nominal thickness of ~8 km [*Baker and Stair*, 1988], the temperatures provided by the TIMED/SABER team are kinetic temperatures representative of a certain altitude at a vertical resolution of ~2 km [*Mertens et al.*, 2004]. To make a realistic comparison, the kinetic temperatures have to be weighted over the OH emission layer to be equivalent to the ground-based temperatures. *Mulligan and Lowe* [2008] present several methods to do this, and in this paper we calculate so-called OH brightness temperatures using the OH 1.6 μm volume emission rate (VER) measured simultaneously by SABER to weight the kinetic temperature profiles derived from measurements of CO_2 emissions made by SABER [*Mertens et al.*, 2004]. The OH 1.6 μm VER signal covers the spectral interval 1.56–1.75 μm and thus includes most of the $\Delta\nu = 2$ bands OH(4-2) and OH(5-3). OH brightness temperatures were calculated from each SABER temperature profile that satisfied certain coincidence criteria with the Longyearbyen data. Spatially, this means SABER profiles with a tangent point at an altitude of 87 ± 8 km that have geographic coordinates within 78 ± 5°N, 16 ± 10°E (this corresponds to a circle of approximately 600 km centered on the observing site at Longyearbyen). The spatial coincidence criteria were chosen on the basis of the need to secure a certain number of coinciding data and the knowledge of the anomalously low OH peak altitude occurring during this particular season [*Winick et al.*, 2009]. SABER measurements that fell within the same day were used to compute the daily averaged SABER temperature that we could compare with our daily averaged OH(6-2) temperatures. The effect of choosing a narrower temporal coincidence criterion is discussed further in section 3.

[10] In the following description, we will use the phrase "SABER temperatures" to refer to OH brightness temperatures derived from temperature profiles produced by version 1.07 of the SABER analysis software. The SABER kinetic temperatures and OH 1.6 μm VER data were downloaded from http://saber.gats-inc.com. Like earlier versions of SABER data, version 1.07 does not routinely provide individual error estimates for the kinetic temperatures. The resulting daily averaged SABER temperatures from 2003 to 2004 are shown in dark blue in Figure 1 (top). As for the OH(6-2) temperatures, the error bars are the standard deviation of the individual measurements comprising the daily mean. These errors are influenced mainly by atmospheric variability. Alternatively, we could have used the overall uncertainty of the kinetic temperature measurements as error bars. The error in kinetic temperatures for mesopause heights at polar winter was estimated by *Remsberg et al.* [2008] for the version 1.07 data. They report an estimate of the combined systematic and relative errors of ~5 K. That would have left us with equal error bars of ±5 K for all the daily averaged temperatures. This needs to be kept in mind when interpreting the SABER temperatures in Figure 1.

[11] From the OH VER profiles, the altitude of the emission layer and the integrated rate of emission can be computed. The peak altitude was chosen to be the peak altitude of the Gaussian that best fit the measured OH VER profile, following the method that *Liu and Shepherd* [2006] used when analyzing Wind Imaging Interferometer (WINDII) satellite data. Figure 1 (middle) displays daily averaged OH peak altitudes from 2003 to 2004. The error bars show the standard deviation of the daily mean as explained in the previous section and indicate mainly atmospheric variability. The corresponding integrated emission rate was obtained by computing the integral of the area under the OH VER profiles.

[12] Zonal and meridional winds at the mesopause level were obtained from analysis of meteor echoes measured by the NSMR. The NSMR is of the type often referred to as a meteor wind radar (MWR) or recently simply as a meteor radar. The system operates at 31 MHz and is colocated with the ground-based optical instruments at Longyearbyen. A description of the system is given by *Hall et al.* [2002] and *Holdsworth et al.* [2004]. MWRs illuminate a large region of the sky, and echoes from meteor trains are detected by receivers arranged as an interferometer. Descriptions of how winds are determined are given by *Aso et al.* [1979], *Hocking et al.* [2001], and *Tsutsumi et al.* [1999]. A MWR at high latitude suffers less from strong diurnal variation of meteor rate than one does at low latitude, and therefore it is possible to obtain a time resolution of 30 min for a whole day. The resulting 30 min average winds represent, however, a spatial averaging over perhaps 200 km at the peak echo occurrence height of 90 km. For this study the measured wind data have been averaged over bins spanning 1 day and 2 km in height in the altitude range 70–100 km. Figure 1 (bottom) shows zonal and meridional winds for the altitude range 74–100 km.

3. Comparison of OH(6-2) and SABER Temperatures

[13] The SABER and OH(6-2) daily averaged temperatures for the 2003–2004 winter season are shown in Figure 1 (top) in dark blue and green, respectively. As noted earlier, the error bars indicate the standard deviation from the mean and are mainly influenced by atmospheric variability. There are no SABER temperatures available from mid November to mid January. This is because the yaw periods of the satellite are such that it spends 60 days looking northward followed by 60 days looking southward. The southward looking 60 days are approximately day 325 of year n until day 15 of year $n + 1$. Unfortunately, this coincides with the main period of observation for the ground-based spectrometer in Longyearbyen. Due to exceptionally good observing conditions, an unusually large number of OH(6-2) temperatures were available for analysis in the period 16 January–19 February 2004, when SABER was looking northward [*Dyrland and Sigernes*, 2007]. This allowed us to make a comparison of the two temperature sets despite the disadvantageous SABER yaw cycle.

[14] From Figure 1 (top) it is clear that the relative variations of the SABER and OH(6-2) temperatures are similar. The mean daily averaged temperature for the overlapping data (31 days in mid November and January–February) is 244.1 ± 14.1 K for SABER and 238.5 ± 12.6 K for OH(6-2). The error indicates the standard deviation from the mean. This gives a mean difference, $\overline{T_{SABER} - T_{OH(6-2)}}$, of 5.6 ± 4.4 K. The margin of error for the mean offset was estimated using a paired t test [*Moore and McCabe*, 1999] for a confidence level of 95%. The linear correlation coefficient between the daily averaged temperature series is 0.605, with a probability of random occurrence of $<10^{-3}$. To test whether the positive offset for SABER could be due to differences in sampling time for the two instruments, the temporal coincidence criterion was shortened. Only SABER data that fell within the 1 hour integrated OH(6-2) spectra were chosen. This resulted in 100 temperatures within the 31 coinciding days. The mean offset is still positive but is increased to 8.4 ± 3.4 K. Again, the error for the mean offset was estimated using a paired t test [*Moore and McCabe*, 1999] for a confidence level of 95%. Both of these offsets are within the combined uncertainties of the two data sets, and we conclude that the two time series correspond well enough for us to regard them as a continuous temperature series from the 2003–2004 winter. Although not the main theme in this paper, we will discuss possible reasons for the observed positive offset in the following paragraphs.

[15] Several authors have compared SABER data with OH temperatures measured from low and middle latitudes. Most have found the SABER equivalent temperature to be colder than the rotational temperature by 4–9 K [e.g., *Oberheide et al.*, 2006; *López-Gonzales et al.*, 2007; *Mulligan and Lowe*, 2008], that is, the opposite of what we see from our data. To our knowledge no thorough comparison of SABER and rotational OH temperatures from high Arctic latitudes has been reported. However, from Figure 1 in the paper by *Siskind et al.* [2005] we see that SABER are higher than rotational OH(4-2) temperatures measured at Rothera, Antarctica (67.6°S, 68.1°W), by an average of ~4 K. This observed offset is also positive in favor of SABER, although it is a bit smaller than the offset reported here. Although our data set and theirs are obviously too small to substantiate a general positive bias for SABER, the fact that we find the opposite of what others have found at middle and lower latitudes is very interesting. A future investigation could examine other comparisons of SABER temperatures with rotational temperatures derived from OH spectra to check whether the high-latitude bias observed in the two cases is sustained.

[16] There are several factors that might explain the positive offset for SABER observed for our 31 days of data. The SABER temperatures are kinetic temperatures from CO_2 weighted by profiles of OH volume emission rates from the OH(4-2) and OH(5-3) bands, whereas the OH(6-2) values are rotational temperatures. Using spectra from high-resolution spectrographs mounted at the Keck 1 and Keck 2 telescopes on Mauna Kea and the Kueyen telescope in Chile, *Cosby and Slanger* [2007] showed that OH rotational temperatures can differ by as much as 20 K when different bands are used. In addition, the peak height and vertical distribution of different vibrational levels of excited OH have been shown to vary with height [*López-Moreno et al.*, 1987]. Higher vibrational levels seem to have their maxima at higher altitude [*Kaufmann et al.*, 2008]. This could imply that the peak of the OH layer found from SABER measurements of the volume emission rates of the OH(4-2) and (5-3) bands are lower than the actual peak altitude of the OH(6-2) emissions. In Figure 2 (left) we see that monthly

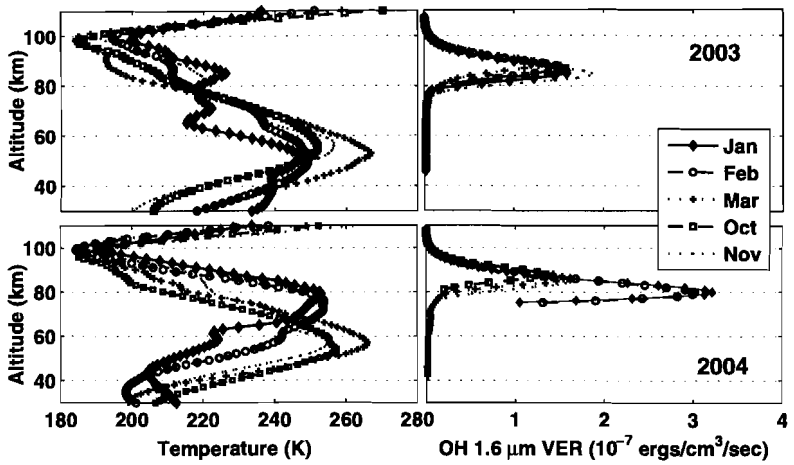

Figure 2. (left) Monthly averaged SABER temperature profiles for January, February, March, October, and November (top) 2003 and (bottom) 2004. Data shown are from the altitude range 30–110 km above Longyearbyen and for a solar zenith angle >105°. (right) Monthly averaged SABER OH volume emission rate (VER)1.6 μm profiles for the same months of (top) 2003 (top panel) and (bottom) 2004.

averaged environmental lapse rates (i.e., observed vertical gradients in the kinetic temperature) measured by SABER during 2003–2004 are of the order of 1.5 K/km. However, higher and also reversed vertical temperature gradients are also observed for selected SABER spectra, indicating that even small differences in the peak altitude among vibrational levels 4, 5, and 6 may be part of the reason for the observed differences between SABER and the OH(6-2) temperatures. This could also possibly explain why *Siskind et al.* [2005], who used temperatures from the OH(4-2) band, find a smaller offset than we do. In addition, lower vibrational OH emission profiles have been shown to be generally broader than those of the higher levels due to the more efficient quenching of the latter at lower altitudes [*Makhlouf et al.*, 1995]. This and the fact that the ratio between emission rates of different vibrational levels is not constant during the day may also contribute to differences between the SABER and OH(6-2) temperatures [*Cosby and Slanger*, 2007, and references therein].

[17] The temperatures calculated for a certain band also clearly depend on the choice of transition coefficients. The values of *Goldman et al.* [1998] used in our analysis yield about 6.5 K higher temperatures than the values of, for example, *Langhoff et al.* [1986]. Use of the latter coefficients thus increases the mean positive offset of SABER temperatures. The difference in fields of view of the two instruments is probably one of the main reasons for differences in the relative variation. OH(6-2) spectra are obtained from a spectrometer that views in the zenith and has a horizontal field of view of approximately 9 km × 12 km at 90 km altitude [*Viereck and Deehr*, 1989], and the spectra are integrated vertically. The SABER instrument has a 2 km vertical resolution and a horizontal field of view of about 200 km × 20 km [*Oberheide et al.*, 2006].

[18] Unfortunately, no other season had such a long overlap period between SABER and spectrometer measurements as 2003–2004, but from 25 January to 4 February 2003 there were 9 days when the two coincided. The mean OH layer temperature for that time period was 212 ± 7 K and 203 ± 14 K for SABER and OH(6-2) temperatures, respectively. The mean positive offset for SABER is 9 ± 11 K. Thus we find that even in the case of a "normal" year, the SABER temperatures are generally warmer than the ground-based measurements. However, note that this is not a significant bias at a 95% confidence level since the estimated error is larger than the actual bias. More important, as we have already noted, the warm offset for the SABER temperatures are within the uncertainties of the two measurement techniques. We therefore conclude that the two series correspond well and that viewing them in combination as a near-continuous temperature series from the 2003–2004 winter is reasonable.

4. Temperature and Wind Variations During 2003–2004

[19] To understand the temperature variations of the 2003–2004 winter it is critical to have information about the altitude of the OH emission layer [*Kumar et al.*, 2008]. The daily averaged OH layer peak altitudes corresponding to the SABER temperatures are plotted in Figure 1 (middle). Figure 1 (bottom) shows the NSMR zonal and meridional winds. We divide the winter into three different periods according to the characteristics of the OH layer.

[20] We first look at the period from 25 October to 3 December 2003, period 1 in Figure 1. During the start of this period the OH temperature was relatively low (~200 K) but increased from 1 November. The low temperatures coincided with an equatorward meridional wind. On a global scale, equatorward meridional winds are coupled to upwelling and adiabatic cooling over the poles, and this has been shown to be coupled to airglow variability as well [*Shepherd et al.*, 2006]. Looking at Figure 1 (top and middle), it is clear that the rise in temperatures of about 35 K during the 14 day period after 1 November coincided with a reduction in the altitude of the OH layer peak of 5 km. Unfortunately, wind measurements are not available for most of this event. We can, however, get a clue by looking at the

period 11–14 November, during which the zonal wind was eastward and the meridional wind was poleward below 90 km, consistent with downwelling and adiabatic warming. After 14 November the temperature decreased somewhat, and the meridional wind turned equatorward. Although local-scale winds like those measured by NSMR do not necessarily correspond to the global-scale winds believed to influence the downwelling/upwelling over the Arctic, it is intriguing that an apparent correlation between meridional winds and airglow temperature and peak altitude is observed. We discuss this more thoroughly in section 5.

[21] In period 2 (see Figure 1), from 4 December 2003 to 8 January 2004, the OH temperature decreased rapidly by ~40 K during the first few days. Unfortunately, there are no meteor radar wind or SABER data available for this period. However, *Mukhtarov et al.* [2007] report a similar negative excursion of the ~90 km temperature starting around 1 December, indicating that it is not just a local feature. They attribute it to strong disturbances in the mean zonal wind in the mesopause region (80–90 km) seen in radar measurements averaged for 60°N –70°N. According to them, these are actually the first signs of the enhanced planetary wave activity that led to the major SSW occurring in late December to early January. The actual reversal of the stratospheric zonal wind at 60°N and thus onset of the SSW occurred on 2 January 2004 [*Manney et al.*, 2005]. *Mukhtarov et al.* [2007] identified it occurring 10–14 days earlier in ~80 km winds measured by radars at 63°N –69°N. So in a way there seem to be two dates that can be associated with the onset of the SSW in the MLT/mesopause region: one around 4 December associated with enhanced planetary wave activity that is believed to be the driver of the SSW event, and one around 24 December, when the zonal wind reversed again. We have already discussed the signatures in the OH temperatures for the first event. The temperature data around 24 December do not reveal a similar large decrease of temperature, although several negative excursions on the order of 20 K are seen around that time. However, looking at the wind data, we observe that from 15 to 23 December the zonal wind is mainly eastward, while it reverses and is westward at 26–28 December. This is consistent with the expected signature of the SSW in this region. The data gaps are especially unfortunate in this period since they make it difficult to assign changes in OH temperature and winds to the SSW, but at least we can show that the general picture drawn by *Mukhtarov et al.* [2007] is also valid for our latitude. The temperature remained relatively low for the rest of this period, and the equatorward meridional wind observed is consistent with this.

[22] Period 3 (see Figure 1), from 9 January to 7 March 2004, is the most interesting period of this winter. We believe that the westward wind seen in Figure 1 (bottom) from 9 to 12 January is likely to be the remains of the wind reversal at mesopause level associated with the SSW and stratospheric vortex disruption. This corresponds well with the recovery of the upper stratospheric vortex and onset of eastward wind by 18 January reported by *Manney et al.* [2005]. The vortex remained strong until mid March. SABER and OH(6-2) temperatures increased and remained high during this period. The zonal and meridional winds changed direction at 13 January from westward/equatorward to eastward/poleward, which is consistent with a reestablishment of the polar vortex. This occurred around the same time as the OH(6-2) temperature began to increase. The OH layer peak altitude shown in Figure 1 (middle) decreased at the beginning of period 3 and remained low until 22 February. The reduction in temperature and corresponding rise of the OH layer peak around 1 February is probably associated with the shorter major SSW in late January [*Manney et al.*, 2005]. After 1 February the temperature increased again, achieving values greater than 250 K, and the OH layer peak altitude dropped below 78 km. Unfortunately, there are no OH(6-2) temperatures available after 19 February and no winds after 10 February. The SABER data show that the temperature dropped by about 50 K, and the OH layer peak altitude increased correspondingly, in a very short time near 22 February. The close relationship between OH height and temperature is especially clear here. The large zonal asymmetries in the OH layer temperature, emission, and height reported by *Winick et al.* [2009] would be interesting to study in relation to this abrupt change to see whether temporal or spatial variability, or a combination thereof, is the cause of it. To do this, one would need data from other stations at different longitudes and latitudes.

5. Discussion

[23] To illustrate the OH layer variations observed, we plotted monthly averaged SABER temperature profiles for selected months of 2003 and 2004 in Figure 2 (left). Figure 2 (right) shows the corresponding monthly averaged SABER OH VER 1.6 μm emission profiles. The criterion that the solar zenith angle is >105° ensures that data are obtained during darkness. From the emission profiles it is clear that the OH layer over Longyearbyen during January and February 2004 is very low compared to the more "normal" year of 2003, when the peak altitude was around 87 km and the temperatures were lower. The VER of the OH layer in January and February 2004 is approximately twice its value in the same months of 2003.

[24] The coincidence of high temperatures with a reduction in altitude and an increase in the brightness of the OH layer was observed previously. *Yee et al.* [1997] showed that the peak altitude of the OH emission is inversely correlated with the strength of the emission. This inverse relationship was also observed by *Winick et al.* [2009] in their SABER data from 2003 to 2004. From their data they noted that the OH layer altitude and the temperature at the OH layer are also inversely related. They showed that during the period 26–31 January 2004 the OH layer was not zonally symmetric, and that for high-latitude stations eastward of 50°E the layer showed no unusual behavior. At 16°E, Longyearbyen was approximately halfway between the undisturbed region and the highly disturbed region at 50°W. From our ground-based measurements we can confirm the existence of the unusually low OH layer at the longitude of Longyearbyen.

[25] In a study of the correlation between airglow temperature and emission rate at the high-latitude location Resolute Bay (75°N), *Cho and Shepherd* [2006] found evidence of a common process for all dynamical perturbations of the airglow layer and argued that this process is vertical motion. This is supported by the work of *Marsh et al.* [2006], who compared SABER observations of OH emission

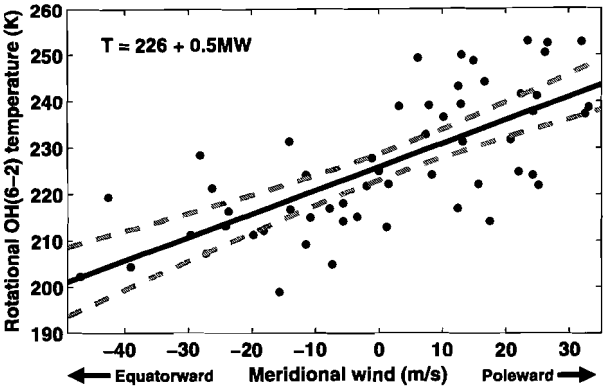

Figure 3. Scatter diagram of the 55 coinciding OH(6-2) temperatures and meridional wind at 84–86 km from Longyearbyen between 17 November 2003 and 11 February 2004. The solid line shows the best least squares linear fit to the data points. The dashed lines indicate the 95% confidence interval for the fit (corresponding to the two-sigma error of the slope and intercept). T denotes the temperature, and MW denotes the value for the meridional wind. The correlation coefficient is 0.71, with the probability of random occurrence of $<10^{-8}$.

rates with a three-dimensional chemical model. They found that at the height of peak emission, variations are predominantly caused by changes in atomic oxygen resulting from vertical transport. This leads to an increase in ozone, which leads to an increase in the band brightness and temperature. The formation of the OH layer at lower altitudes that we observe is also likely to be the result of downwelling of atomic oxygen-rich air to lower heights as suggested by *Winick et al.* [2009].

[26] To get an idea of the quantitative effect of the lowered OH layer on the temperature, we can look at the temperature profiles in Figure 2 (left). From these we see that the environmental lapse rate (observed vertical temperature gradient with decreasing pressure) is approximately 1.5 K/km in the altitude range 60–100 km. Of the 35 K temperature increase observed in the beginning of period 1, we estimate that about 7.5 K is due to the OH layer peak occurring 5 km lower down, according to the environmental lapse rate observed. Correspondingly, of the overall ~50 K increase of temperature from late October to mid February, we ascribe about 15 K to the close to 10 km lowering of the OH layer, as observed in Figure 1 (top and middle). The remaining temperature increase is then attributed to adiabatic heating of the subsiding air and chemical heating due to the exothermic reactions involved in producing the vibrationally excited OH.

[27] The exothermic reaction producing vibrationally excited OH is

$$H + O_3 \xrightarrow{k} OH(v)^* + O_2, \quad (1)$$

with reaction rate coefficient $k = 1.4 \times 10^{-10} e^{-470/T}$ cm^3/ s. It is generally thought of as the largest source of heat in the vicinity of the mesopause [*Mlynczak and Solomon*, 1993]. Chemical heating rates involving this and other processes have been calculated by several authors and mainly range from 2 to 10 K/d and decrease with height from the maximum at ~90 km due to collisional quenching becoming more dominant at lower altitudes [*Mlynczak and Solomon*, 1993; *Kaufmann et al.*, 2008]. However, *Smith et al.* [2003] showed that these rates can increase at altitudes between 78 and 98 km in the presence of tides. They argued that this is mainly due to the net downward advection of atomic oxygen by the tidal vertical motions. According to *Marsh et al.* [2006], a positive correlation between OH airglow emission rate and temperature is indicative of the change in OH emissions being caused by transport of atomic oxygen, not by changes in density and reaction rates. This is because the production of excited OH mainly depends on the production of ozone, which decreases with temperature [*Marsh et al.*, 2006]. Both the spectrometer and SABER data verify the positive correlation between emission rate and temperature in January and February 2004 (daily data not shown) and thus support increased transport of atomic oxygen as the main cause for the anomalously warm temperature, low peak altitude, and increased emission rate observed.

[28] The adiabatic heating of displaced air volumes follows the dry adiabatic lapse rate, which is ~9.5 K/km at mesopause heights [*Sherman and She*, 2006]. Note that the dry adiabatic lapse rate is different from the environmental lapse rate quoted earlier. The latter is the observed vertical temperature gradient, which is a result of the balance between all heating and cooling processes [*Andrews*, 2000]. The main cooling process is radiative cooling by vibrational relaxation in the infrared 15 μm band of CO_2. Typical cooling rates for the 70–90 km region at high Arctic latitudes are 5–20 K/d [*López-Puertas et al.*, 1992]. Seasonal variability and other shorter time scale variations that may also influence the temperature (e.g., planetary waves, gravity waves, and tides) are not quantified here. Ideally we would be able to quantify the relative rates of chemical heating, adiabatic warming, and radiative cooling. However, this is beyond our scope. Instead we will discuss the mechanism responsible for the lowering of the layer and the increased temperatures in view of our wind measurements made by NSMR.

[29] The strong poleward meridional wind observed at the OH layer height (~80 km) during most of period 3 is probably also contributing to the emission intensity level by transporting odd oxygen species from their source region to the high latitudes (where there is no winter production of O by photodissociation [*Myrabø and Deehr*, 1984]), as well as by increasing downwelling, which further increases adiabatic warming. To test for a possible coupling, we calculated the correlation coefficients between daily averaged meridional winds measured by the meteor radar at different heights and the OH(6-2) temperatures for the 55 days that the measurements coincided between 17 November 2003 and 11 February 2004. Table 1 shows the correlation coefficients and probabilities of random occurrence. Figure 3 shows the correspondence between temperature and the wind at 84–86 km height, for which we found the largest correlation. The correlation coefficient is 0.71, with a probability of random occurrence of $<10^{-8}$. This means that around 50% of the variation in temperature can be related to variations in the meridional wind direction and strength. From Figure 3 we see how a poleward wind is consistent

Table 1. Correlation Coefficient R and Probability of Random Occurrence p for the Linear Relationship Between Meridional Wind at Different Heights (70–96 km) and OH(6-2) Temperature, SABER OH Temperature, and SABER OH Peak Altitude[a]

Altitude (km)	MW vs. OH(6-2) T		MW vs. SABER T		MW vs. SABER OH Alt	
	R	p	R	p	R	p
70–72	0.63[b]	6.3E-7	0.59[c]	3.1E-5	−0.66[c]	1.2E-6
72–74	0.62	3.6E-7	0.72	2.9E-8	−0.80	1.5E-10
74–76	0.67	2.3E-8	0.76	2.9E-9	−0.81	3.9E-11
76–78	0.68	8.6E-9	0.78	6.5E-10	−0.83	1.6E-11
78–80	0.70	2.8E-9	0.76	2.0E-9	−0.81	2.8E-11
80–82	0.69	5.1E-9	0.75	5.4E-9	−0.78	5.3E-10
82–84	0.70	2.1E-9	0.74	1.1E-8	−0.73	2.2E-8
84–86	0.71	1.3E-9	0.72	4.4E-9	−0.68	3.6E-7
86–88	0.66	3.6E-8	0.67	7.6E-7	−0.62	7.6E-6
88–90	0.56	8.9E-6	0.56	7.6E-5	−0.51	3.6E-4
90–92	0.46	4.3E-4	0.48	1.1E-3	−0.41	5.1E-3
92–94	0.26	5.1E-2	0.35	1.8E-2	−0.29	6.1E-2
94–96	0.040	7.5E-1	0.30	5.1E-2	−0.24	1.2E-1

[a]For all altitudes except 70–72 km there were 55 coinciding days for spectrometer and meteor radar measurements and 44 coinciding days for the Sounding of the Atmosphere using Broadband Emission Radiometry (SABER) instrument and meteor radar measurements. Abbreviations are as follows: MW, meridional wind; OH Alt, OH peak altitude; T, temperature.
[b]Only 52 coincident days.
[c]Only 43 coincident days.

with a higher temperature, while an equatorward wind gives a lower temperature. A simple linear regression gives the relationship between the OH(6-2) temperature (T) and the meridional wind (MW): $T = 225.9(\pm 2.8) + 0.50(\pm 0.14)$. The margins are the two-sigma errors for the intercept and slope [*Moore and McCabe*, 1999]. The best linear fit is plotted in Figure 3 (solid line) together with its 95% confidence interval (corresponding to the two-sigma error in slope and intercept). The linear relationship is probably indicating a local footprint of gravity wave breaking in the mesosphere, which modulates the zonal wind and drives the mean meridional circulation that is responsible for the cold summer and warm winter mesopause temperatures at high latitudes [*Garcia and Solomon*, 1985; *Fritts and Alexander*, 2003]. The correlation coefficient found is comparable to the findings of *Espy et al.* [2003], who reported a correlation of −0.61 between meridional wind measured by medium-frequency radar and OH(4-2) rotational temperatures at Rothera, Antarctica. The negative sign of their correlation is due to poleward wind in that hemisphere being defined as negative. They found a slope of −0.71 K/(m/s), comparable to our slope of 0.5 K/(m/s). Our calculations for zonal winds gave a correlation coefficient of only 0.25 and a probability for random occurrence of 0.066. *Espy et al.* [2003] found a correlation of 0.29 between zonal wind and rotational temperatures at Rothera, so these numbers are also of the same order. We believe the correlation is real, despite the relatively high probability of random occurrence, because a westward flow combined with gravity wave drag is expected to produce an equatorward component and vice versa [*Holton*, 1983].

[30] We also calculated the correlation between the meridional wind at different heights and the temperature and altitude of the OH layer measured by SABER for the 44 days the two coincided between 25 October and 11 February. If the poleward meridional wind is a major driver of downward transport and hence adiabatic heating as our data indicate, we can also expect it to have a role in bringing more oxygen-rich air to lower altitudes and thus lowering the OH peak altitude. Table 1 shows the correlation coefficient R between the meridional wind at different heights and OH(6-2) temperature, SABER OH temperature, and SABER OH peak altitude. The corresponding probabilities of random occurrence, p, are also listed. It is interesting to see that the maximum correlation with the SABER measurements was found for winds at 76–78 km height, not higher up as for OH(6-2) temperatures. Figure 4 shows the meridional wind at 76–78 km height plotted against OH layer peak altitude and the least squares linear fit to the data points. The linear relationship found is $Alt_{OH} = 84.8(\pm 0.85) - 0.13(\pm 0.03)$ MW, where Alt_{OH} is the peak altitude of the OH layer and MW is the strength of the meridional wind. The error margins in Figure 4 are the two-sigma errors of the intercept and slope of the best fit [*Moore and McCabe*,

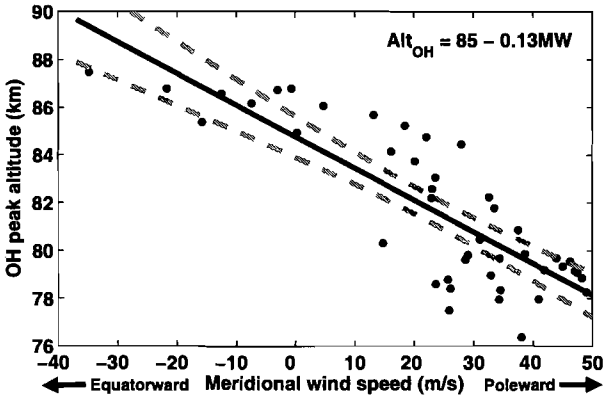

Figure 4. Scatter diagram of the 44 coinciding OH peak altitudes measured by SABER and meridional wind at 76–78 km from Longyearbyen between 25 October 2003 and 11 February 2004. The solid line shows the best least squares linear fit to the data points. The dashed lines indicate the 95% confidence interval for the fit (corresponding to the two-sigma error of the slope and intercept). Alt_{OH} denotes the peak altitude of the OH layer, and MW denotes the value for the meridional wind. The correlation coefficient is −0.83, with the probability of random occurrence of $<10^{-11}$.

1999]. The dashed lines indicate the corresponding 95% confidence interval of the linear fit. The correlation coefficient is −0.83, with a probability of random occurrence of $<10^{-11}$. This means that more than 68% of the variation in OH layer height can be explained by the meridional wind fluctuations. A 10 m/s increase of meridional wind strength in the poleward direction corresponds to a decrease of OH peak altitude of ~1.3 km, according to our data and the linear relationship found. The quantity of data is clearly not sufficient to treat this as a general rule, but it is indicative of the relation between the two parameters. To our knowledge it is the first time a significant linear correlation between meridional wind strength and OH layer peak altitude has been observed. The meteor radar, spectrometer, and satellite data are three completely independent measurements, and having them probe the same region gives new possibilities for interpreting the different data sets. The strength of the meridional winds seems to be an important key in the OH airglow budget, not only by transporting atomic oxygen from the source region to the high-latitude regions, but also due to its close connection with downwelling of atomic oxygen (decreasing the OH layer peak height and increasing the chemical heating) and by inducing adiabatic heating/cooling of the neutral air.

[31] Our data support the theory that there is a coupling between the strong polar vortex observed at the upper stratosphere during period 3 and the anomalously high OH temperatures and low OH-layer peak altitudes. *Siskind et al.* [2007] provided a potential explanation for the mechanism responsible for bringing atomic oxygen-rich air to unusually low altitudes, and *Winick et al.* [2009] discussed it in the context of their SABER measurements of version 1.06 OH temperatures, altitudes, and peak VER. A strong stratospheric vortex confines air to the polar region and leads to unmixed descent of oxygen-rich air to lower altitudes. At the same time, the disturbed warm lower stratosphere blocks propagation of gravity waves, which normally break near the stratopause and warms this region. The temperature profiles for January and February 2004 in Figure 2 show that this was a likely state for the atmosphere above Longyearbyen. The ~50 km region for January and February 2004 was cold, while the stratopause is as high as 75–80 km. A recent model study by *Karlsson et al.* [2009] also attributed high temperatures at 80 km to enhanced downwelling that results from the negative gravity wave drag associated with weak planetary wave activity in the lower atmosphere. They also suggested interhemispheric coupling mechanisms between temperature and wind fields. That coupling would be interesting to investigate by combining our data sets with those at other latitudes and longitudes.

6. Summary

[32] For the Arctic winter of 2003–2004, we have assembled a detailed picture of the behavior of OH temperatures and peak altitudes from a combination of ground-based and satellite data. The SABER temperatures and OH(6-2) rotational temperatures display similar relative variations. A positive offset of 5.6 ± 4.4 K is found in favor of SABER when compared to rotational temperatures, which is opposite to the sign found at lower latitudes. Differences in peak altitude and rotational distribution of different vibrational bands and differences in fields of view of the satellite and ground-based instruments are suggested as possible explanations for the offset observed. Since the offset is within the combined uncertainties of the two measurements, we considered them together as a near-continuous temperature record from the 2003–2004 winter. This allowed us to describe the evolution of the winter at mesopause level from late October to early March.

[33] By studying the temperature and wind record from 2003 to 2004, we have identified the signatures of the SSW at the mesopause region above Longyearbyen. The reversal of the zonal wind occurred approximately 24 December 2003, around 10 days earlier than the reversal in the stratosphere. The eastward wind was reestablished after 13 January 2004, and around the same time the temperature increased dramatically and remained high until late February. In the same period the OH layer peak altitude was anomalously low. Studies of the correlation between meridional wind at different heights and OH temperature and altitude reveal a close relationship. About 50% of the variation of the OH(6-2) temperature can be assigned to variations in meridional wind direction and strength. For the SABER OH temperatures and peak altitudes there is also a clear relationship. Variations in the peak altitude of the OH layer can be attributed to variations in the meridional wind. An increase in the poleward/equatorward wind of 10 m/s corresponds to a lowering/raising of the OH layer by ~1.3 km.

[34] The data presented in this paper support the theory that vertical transport is the mechanism responsible for much of the modulation in OH layer emission and thus the temperature variations observed. This transport was enhanced because of the unique stratospheric conditions during the 2003–2004 winter, when an unusually strong upper stratospheric vortex led to increased descent of atomic oxygen, which has a key role in OH chemistry. Of the observed temperature increase of ~50 K during the 2003–2004 winter, the re-formation of the OH layer at approximately 10 km below its nominal altitude of 87 km accounted for a temperature increase of ~15 K. The remainder (20–35 K) was due to adiabatic and chemical heating resulting from the increased downwelling coupled to the strong meridional winds observed and other unidentified processes.

[35] Our study confirms the importance of having information about the OH layer altitudes at hand when analyzing rotational temperature time series obtained from ground-based or satellite instruments. The satellite data have been invaluable in this sense, as they provide an independent measurement of the OH layer properties. This knowledge also opens up the possibility to use meridional wind direction and strength as a predictor of temperature and OH layer peak heights, but analysis of a much larger data set is needed to explore this possibility.

[36] **Acknowledgments.** We are very grateful to the entire NASA TIMED/SABER team for making the SABER data freely available. We also thank the three anonymous reviewers for their constructive comments and suggestions, which helped improve the paper.

References

Andrews, D. G. (2000), *An Introduction to Atmospheric Physics*, 229 pp., Cambridge Univ. Press, Cambridge, U. K.

Andrews, D. G., J. R. Holton, and C. B. Leovy (1987), *Middle Atmosphere Dynamics*, 489 pp., Academic, San Diego, Calif.

Aso, T., T. Tsuda, and S. Kato (1979), Meteor radar observations at Kyoto University, *J. Atmos. Terr. Phys.*, *41*, 517–525, doi:10.1016/0021-9169(79)90075-8.

Baker, D. J., and A. T. Stair Jr. (1988), Rocket measurements of the altitude distributions of the hydroxyl airglow, *Phys. Scr.*, *37*, 611–622, doi:10.1088/0031-8949/37/4/021.

Beig, G., et al. (2003), Review of mesospheric temperature trends, *Rev. Geophys.*, *41*(4), 1015, doi:10.1029/2002RG000121.

Bevington, B. R., and D. K. Robinson (1992), *Data Reduction and Error Analysis for the Physical Sciences*, 328 pp., McGraw-Hill, New York.

Cho, Y.-M., and G. G. Shepherd (2006), Correlation of airglow temperature and emission rate at Resolute Bay (74.68°N), over four winters (2001–2005), *Geophys. Res. Lett.*, *33*, L06815, doi:10.1029/2005GL025298.

Cosby, P. C., and T. G. Slanger (2007), OH spectroscopy and chemistry investigated with astronomical sky spectra, *Can. J. Phys.*, *85*, 77–99, doi:10.1139/P06-088.

Dyrland, M. E., and F. Sigernes (2007), An update on the hydroxyl airglow temperature record from the Auroral Station in Adventdalen, Svalbard (1980–2005), *Can. J. Phys.*, *85*, 143–151, doi:10.1139/P07-040.

Espy, P. J., R. E. Hibbins, G. O. L. Jones, D. M. Riggins, and D. C. Fritts (2003), Rapid, large-scale temperature changes in the polar mesosphere and their relationship to meridional flows, *Geophys. Res. Lett.*, *30*(5), 1240, doi:10.1029/2002GL016452.

Fritts, D. C., and M. J. Alexander (2003), Gravity wave dynamics and effects in the middle atmosphere, *Rev. Geophys.*, *41*(1), 1003, doi:10.1029/2001RG000106.

Garcia, R. R., and S. Solomon (1985), The effect of gravity waves on the dynamics and chemical composition of the mesosphere and lower thermosphere, *J. Geophys. Res.*, *90*, 3850–3868, doi:10.1029/JD090iD02p03850.

Goldman, A., W. G. Schoenfeld, D. Goorvitch, C. Chackerian Jr., H. Dothe, F. Mélen, M. C. Abrams, and J. E. A. Selby (1998), Updated line parameters for OH $X^2\Pi$-$X^2\Pi$ (v'',v') transitions, *J. Quant. Spectrosc. Radiat. Transf.*, *59*(3–5), 453–469, doi:10.1016/S0022-4073(97)00112-X.

Hall, C. M., T. Aso, and M. Tsutsumi (2002), An examination of high latitude upper mesosphere dynamic stability using the Nippon/Norway Svalbard Meteor Radar, *Geophys. Res. Lett.*, *29*(8), 1211, doi:10.1029/2001GL013894.

Hocking, W. K., B. Fuller, and B. Vandepeer (2001), Real-time determination of meteor-related parameters utilizing modern digital technology, *J. Atmos. Sol. Terr. Phys.*, *63*, 155–169, doi:10.1016/S1364-6826(00)00138-3.

Hoffmann, P., W. Singer, D. Keuer, W. K. Hocking, M. Kunze, and Y. Murayama (2007), Latitudinal and longitudinal variability of mesospheric winds and temperatures during stratospheric warming events, *J. Atmos. Sol. Terr. Phys.*, *69*, 2355–2366, doi:10.1016/j.jastp.2007.06.010.

Holdsworth, D. A., I. M. Reid, and M. A. Cervera (2004), Buckland Park all-sky interferometric meteor radar, *Radio Sci.*, *39*, RS5009, doi:10.1029/2003RS003014.

Holton, J. R. (1983), The influence of gravity wave breaking on the general circulation of the middle atmosphere, *J. Atmos. Sci.*, *40*, 2497–2507, doi:10.1175/1520-0469(1983)040<2497:TIOGWB>2.0.CO;2.

Karlsson, B., C. McLandress, and T. G. Shepherd (2009), Inter-hemispheric mesospheric coupling in a comprehensive middle atmosphere model, *J. Atmos. Sol. Terr. Phys.*, *71*, 518–530, doi:10.1016/j.jastp.2008.08.006.

Kaufmann, M., C. Lehmann, L. Hoffmann, B. Funke, M. López-Puertas, C. v. Savigny, and M. Riese (2008), Chemical heating rates derived from SCIAMACHY vibrationally excited OH limb emission spectra, *Adv. Space Res.*, *41*, 1914–1920, doi:10.1016/j.asr.2007.07.045.

Kumar, K. K., C. Vineeth, T. M. Antonita, T. K. Pant, and R. Sridharan (2008), Determination of day-time OH emission heights using simultaneous meteor radar, day-glow photometer and TIMED/SABER observations over Thumba (8.5°N, 77°E), *Geophys. Res. Lett.*, *35*, L18809, doi:10.1029/2008GL035376.

Langhoff, S. R., H.-J. Werner, and P. Rosmus (1986), Theoretical transition probabilities for the OH Meinel system, *J. Mol. Spectrosc.*, *118*, 507–529, doi:10.1016/0022-2852(86)90186-4.

Liu, G., and G. G. Shepherd (2006), An empirical model for the altitude of the OH nightglow emission, *Geophys. Res. Lett.*, *33*, L09805, doi:10.1029/2005GL025297.

López-Gonzalez, M. J., et al. (2007), Ground-based mesospheric temperatures at mid-latitude derived from O_2 and OH airglow SATI data: Comparison with SABER measurements, *J. Atmos. Sol. Terr. Phys.*, *69*, 2379–2390, doi:10.1016/j.jastp.2007.07.004.

López-Moreno, J. J., R. Rodrigo, F. Moreno, M. López-Puertas, and A. Molina (1987), Altitude distribution of vibrationally excited states of atmospheric hydroxyl at levels $v = 2$ to $v = 7$, *Planet. Space Sci.*, *35*(8), 1029–1038, doi:10.1016/0032-0633(87)90007-9.

López-Puertas, M., M. A. López-Valverde, and F. J. Taylor (1992), Vibrational temperatures and radiative cooling of the CO_2 15 μm bands in the middle atmosphere, *Q. J. R. Meteorol. Soc.*, *118*, 499–532, doi:10.1256/smsqj.50505.

Makhlouf, U. B., R. H. Picard, and J. R. Winick (1995), Photochemical-dynamical modeling of the measured response of airglow to gravity waves 1. Basic model for OH airglow, *J. Geophys. Res.*, *100*, 11,289–11,311, doi:10.1029/94JD03327.

Manney, G. L., K. Krüger, J. L. Sabutis, S. A. Sena, and S. Pawson (2005), The remarkable 2003–2004 winter and other recent warm winters in the Arctic stratosphere since the late 1990s, *J. Geophys. Res.*, *110*, D04107, doi:10.1029/2004JD005367.

Marsh, D. R., A. K. Smith, M. G. Mlynczak, and J. M. Russel III (2006), SABER observations of the OH Meinel airglow variability near the mesopause, *J. Geophys. Res.*, *111*, A10S05, doi:10.1029/2005JA011451.

Mertens, C. J., et al. (2004), SABER observations of mesospheric temperatures and comparisons with falling sphere measurements taken during the 2002 summer MacWAVE campaign, *Geophys. Res. Lett.*, *31*, L03105, doi:10.1029/2003GL018605.

Mlynczak, M. G., and S. Solomon (1993), A detailed evaluation of the heating efficiency in the middle atmosphere, *J. Geophys. Res.*, *98*, 10,517–10,541, doi:10.1029/93JD00315.

Moore, D. S., and G. P. McCabe (1999), *Introduction to the Practice of Statistics*, 3rd ed., W. H. Freeman, New York.

Mukhtarov, P., D. Pancheva, B. Andonov, N. J. Mitchell, E. Merzlyakov, W. Singer, W. Hocking, C. Meek, A. Manson, and Y. Murayama (2007), Large-scale thermodynamics of the stratosphere and mesosphere during the major stratospheric warming in 2003/2004, *J. Atmos. Sol. Terr. Phys.*, *69*, 2338–2354, doi:10.1016/j.jastp.2007.07.012.

Mulligan, F. J., and R. P. Lowe (2008), OH-equivalent temperatures derived from ACE-FTS and SABER temperature profiles: A comparison with OH*(3–1) temperatures from Maynooth (53.2N, 6.4W), *Ann. Geophys.*, *26*, 795–811.

Myrabø, H. K., and C. S. Deehr (1984), Mid-winter hydroxyl night airglow emission intensities in the northern polar region, *Planet. Space Sci.*, *32*(3), 263–271, doi:10.1016/0032-0633(84)90162-4.

Oberheide, J., D. Offermann, J. M. Russell III, and M. G. Mlynczak (2006), Intercomparison of kinetic temperature from 15 μm CO_2 limb emissions and OH*(3,1) rotational temperature in nearly coincident air masses: SABER, GRIPS, *Geophys. Res. Lett.*, *33*, L14811, doi:10.1029/2006GL026439.

Remsberg, E. E., et al. (2008), Assessment of the quality of the version 1.07 temperature-versus-pressure profiles of the middle atmosphere from TIMED/SABER, *J. Geophys. Res.*, *113*, D17101, doi:10.1029/2008JD010013.

Schoeberl, M. R. (1978), Stratospheric warmings: Observations and theory, *Rev. Geophys. Space Phys.*, *16*, 521–538, doi:10.1029/RG016i004p00521.

Shepherd, G. G., Y.-M. Cho, G. Liu, M. G. Shepherd, and R. G. Roble (2006), Airglow variability in the context of the global mesospheric circulation, *J. Atmos. Sol. Terr. Phys.*, *68*, 2000–2011, doi:10.1016/j.jastp.2006.06.006.

Shepherd, M. G., D. L. Wu, I. N. Fedulina, S. Gurubaran, J. M. Russell, M. G. Mlynczak, and G. G. Shepherd (2007), Stratospheric warming effects on the tropical mesospheric temperature field, *J. Atmos. Sol. Terr. Phys.*, *69*, 2309–2337, doi:10.1016/j.jastp.2007.04.009.

Sherman, J. P., and C.-Y. She (2006), Seasonal variation of mesopause region wind shears, convective and dynamic instabilities above Fort Collins, CO: A statistical study, *J. Atmos. Sol. Terr. Phys.*, *68*, 1061–1074, doi:10.1016/j.jastp.2006.01.011.

Sigernes, F., N. Shumilov, C. S. Deehr, K. P. Nielsen, T. Svenøe, and O. Havnes (2003), The hydroxyl rotational temperature record from the Auroral Station in Adventdalen, Svalbard (78°N, 15°E), *J. Geophys. Res.*, *108*(A9), 1342, doi:10.1029/2001JA009023.

Siskind, D. E., L. Coy, and P. Espy (2005), Observations of stratospheric warmings and mesospheric coolings by the TIMED SABER instrument, *Geophys. Res. Lett.*, *32*, L09804, doi:10.1029/2005GL022399.

Siskind, D. E., S. D. Eckermann, L. Coy, J. P. McCormack, and C. E. Randall (2007), On recent interannual variability of the Arctic winter mesosphere: Implications for tracer descent, *Geophys. Res. Lett.*, *34*, L09806, doi:10.1029/2007GL029293.

Sivjee, G. G., and R. M. Hamwey (1987), Temperature and chemistry of the polar mesopause OH, *J. Geophys. Res.*, *92*, 4663–4672, doi:10.1029/JA092iA05p04663.

Smith, A. K., D. R. Marsh, and A. C. Szymczak (2003), Interaction of chemical heating and the diurnal tide in the mesosphere, *J. Geophys. Res.*, *108*(D5), 4164, doi:10.1029/2002JD002664.

Tsutsumi, M., D. Holdsworth, T. Nakamura, and I. Reid (1999), Meteor observations with an MF radar, *Earth Planets Space*, *51*, 691–699.

Viereck, R. A., and C. S. Deehr (1989), On the interaction between gravity waves and the OH Meinel (6–2) and the O_2 atmospheric bands in the polar night airglow, *J. Geophys. Res.*, *94*, 5397–5404, doi:10.1029/JA094iA05p05397.

Walterscheid, R. L., G. G. Sivjee, and R. G. Roble (2000), Mesospheric and lower thermospheric manifestations of a stratospheric warming event over Eureka, Canada (80°N), *Geophys. Res. Lett.*, *27*, 2897–2900, doi:10.1029/2000GL003768.

Winick, J. R., P. P. Wintersteiner, R. H. Picard, D. Esplin, M. G. Mlynczak, J. M. Russell III, and L. L. Gordley (2009), OH layer characteristics during unusual boreal winters of 2004 and 2006, *J. Geophys. Res.*, *114*, A02303, doi:10.1029/2008JA013688.

Yee, J. H., G. Crowley, R. G. Roble, W. R. Skinner, M. D. Burrage, and P. B. Hays (1997), Global simulations and observations of O(1S), $O_2(1\Sigma)$ and OH mesospheric nightglow emissions, *J. Geophys. Res.*, *102*, 19,949–19,968, doi:10.1029/96JA01833.

C. S. Deehr, Geophysical Institute, University of Alaska Fairbanks, 903 Koyukuk Drive, Fairbanks, AK 99775, USA.

M. E. Dyrland (corresponding author) and F. Sigernes, The University Centre in Svalbard, P.O. Box 156, N-9171 Longyearbyen, Norway. (margit.dyrland@unis.no)

C. M. Hall, Tromsø Geophysical Observatory, University of Tromsø, N-9037 Tromsø, Norway.

F. J. Mulligan, Department of Experimental Physics, National University of Ireland, Maynooth, Ireland.

M. Tsutsumi, National Institute of Polar Research, 10-3, Midoricho, Tachikawa, Tokyo 190-8518, Japan.